# ON SPATIAL DEPENDENCY IN MOLECULAR DISTRIBUTED DETECTION

*Uri Rogers, Tobias Cain, and Min-Sung Koh*

School of Computing and Engineering Sciences, Eastern Washington University, Cheney, WA 99004 USA

## ABSTRACT

This paper explores *in vivo* disease detection by nanomachines sensing signature biomarkers in an aqueous medium via the principles of molecular distributed detection from a theoretical perspective. The biomarker propagation model is based on solutions to the *Fokker-Plank* equation, where comparisons in model accuracy between one-dimensional and three-dimesional variants are compared and contrasted. The impact of biomarker absorption by the nanomachines and the subsequent nonlinear spatial dependence induced will also be discussed relative to optimal distributed detection performance.

***Index Terms*—Molecular Distributed Detection, MDD, Dependent Observations.**

## I. INTRODUCTION

The use of nanomachines for the *in vivo* detection, localization and possible treatment of disease in the human body, such as cancer, has been a vision of both science fiction (Fantastic Voyage, 1966) and medical research for decades [1]–[5]. Today, nanomachines capable of such aspirations are looking less like science fiction and more like a real possibility [6]. With that said, establishing an *in vivo* network to link these nanomachines remains an open research topic, predominantly driven by the fact that wireless communication at nano-scale dimensions is not feasible. There have been numerous proposals to address this challenge, including molecular communication (MC) and acoustic signaling [5], [7]–[12], each having benefits and challenges of their own.

Another significant research opportunity is the actual nanomachine disease detection process. There are some cases where the disease emits biomarkers or signature molecules that are relatively rare [3], and others where the biomarker emissions are similar to naturally occurring biomarkers, such as vascular endothelial growth factor (VEGF) produced by cancerous tumors [13], [14] [14]. Both cases present the opportunity for false positives in the detection scheme, and optimal detection methods represent an open research topic. We explored this topic at an introductory level in [15], and introduced the terminology of molecular distributed detection (MDD).

The goal in [15] was to detect a disease by sensing biomarker emissions that propagate via Brownian motion with laminar flow as shown in Fig. 1. There the nanomachines were assumed to make semi-autonomous decisions regarding the presence of the disease because of a unidirectional communication channel (with the laminar flow) and challenges of MC channel memory [8]. Each nanomachine transmits its local decision molecule to a downstream fusion center (FC) that fuses all collected communication molecules to arrive at a summary decision regarding the disease presence. That work was based on solving the *Fokker-Plank* equation under a set of stringent constraints, including no biomarker absorption, unimpeded propagation model with no reflecting boundaries (e.g., blood vessel wall), and no drift velocity gradient across the vessel diameter. While it is known that the capillary blood flow velocity has a parabolic like shape [16], [17], the work in [18] suggests there is a cell free layer in the capillary with no red blood cells having near single layer laminar flow, where the nanomachines and biomarkers might collect. This implies that assuming zero drift velocity gradient may be appropriate for some *in vivo* observation models. However, the constraints on unimpeded biomarker propagation and no absorption may be over simplistic.

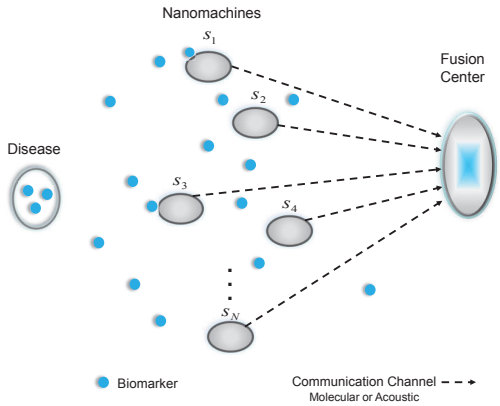


**Fig. 1**. Conceptual MDD system with four key components: 1) Disease releasing molecular biomarkers. 2) $N$ nanomachines. 3) Communication Channel (described in II-A). 4) Fusion Center.

This papers contributions will be to explore how nanomachine biomarker absorption impacts the *in vivo* probabilistic biomarker observation model we proposed in [15]. Absorption results in a hitting-time (e.g., stopping-time) in three dimensional (3-D) space, where no analytical solution to the *Fokker-Plank* equation is known [19]. Because of this, numerical simulation will be used to establish insight into the complexities of this medium, including considerations for using a one dimensional (1-D) hitting-time model in a 3-D space. We will also explore how observations by one nanomachine, can be influenced by a second nanomachine. This results in spatially dependent observations that have a significant impact on MDD disease detection algorithms. In doing so, the following notation will be used: $\triangleq$ is equal by definition, $\Pr(A|B)$ is the probability of event $A$ given event $B$ occurred, $\exists$ is there exists, $\mathbb{R}^n$ is an $n$ dimensional Euclidean space, and $\times$ represents the Cartesian product of sets.

## II. SYSTEM MODEL

A MDD system has a primary goal of determining if a certain disease is present or not, and if so, possibly providing a treatment protocol. These goals require the definition of a MDD model, a nanomachine dependent detection probability model, and a hypothesis testing formulation or fusion rule.

### II-A. Molecular Distributed Detection Model

The conceptual MDD model depicted in Fig. 1 will now be explored in greater detail. There are four primary components that comprise the MDD system model:

1) **Disease**: At a specific location, we assume there is a disease cells that generates a molecular marker (e.g., biomarker such as VEGF [13]) at a given rate, $\kappa$.
2) **Nanomachine**: A collection of biological sized machines labeled as $s_i$, $i = 1, 2, \ldots, N$. Each $s_i$ observes the environment for a biomarker(s), makes a local decision regarding the disease presence every biological clock period $(T_s)$, and then transmits a message to the FC, reflecting that decision. The nanomachines are located down flow from disease and use drift in the aqueous medium to conserve energy until an initial biomarker is detected, where they hold their position until acoustically instructed to move via the FC.
3) **Communication Channel**: Using either MC [9], [15] or acoustic communication similar to that discussed in [5], the nanomachines transmit their local decision to the FC.
4) **Fusion Center**: A nanomachine that fuses the transmitted local nanomachine decisions and makes a summary decision regarding the disease being present or not. It has the ability to acoustically direct the nanomachines operations.

### II-B. Nanomachine Probability Model

Suppose a disease emits a biomarker at some Cartesian coordinate position $\boldsymbol{\xi}_0 = \{x_0, y_0, z_0\}$, with constant emission rate $\kappa$. A single non-interacting biomarker can be modeled in space and time probabilistically using standard Brownian motion via a *stochastic process* $\{\mathcal{B}(t) : t \geq 0\}$, where $\mathcal{B}(t) \in \mathbb{R}^3$ [20]. The probability density function (pdf) for $\mathcal{B}(t)$ can be found using the *Fokker-Plank* (a.k.a. *Kolmogorov Forward*) equation [21]

$$\frac{\partial p_{\mathcal{B}}(t, \boldsymbol{\xi})}{\partial t} = \frac{1}{2} \sum_{j=1}^{3} \sum_{k=1}^{3} \frac{\partial^2 D_{j,k}\, p_{\mathcal{B}}}{\partial \xi_j \partial \xi_k} - \sum_{j=1}^{3} \frac{\partial\, v_j\, p_{\mathcal{B}}}{\partial \xi_j} \tag{1}$$

for $(t, \boldsymbol{\xi}) \in (0, \infty) \times \mathbb{R}^3$, where $p_{\mathcal{B}}(t, \boldsymbol{\xi})$ is a time dependent pdf for an emission at a location $\boldsymbol{\xi}$ and time $t$ starting from the origin at $t = 0$, $D_{j,k}$ are diffusion coefficients, and $v_j$ is the drift velocity in direction $j$. Note, the subscripts on $\xi$ in (1) indicate vector indexes with $\xi_1$ arbitrarily defined as the x-axis in a Cartesian coordinate system. Using the MDD formulation in subsection II-A, we set $D_{j,k} \triangleq 2D_B$ when $j = k$ and zero otherwise for anisotropic diffusion, and set $v_j = v_x$ if $j = 1$ and zero otherwise for single layer laminar flow.

Under certain constraints [20, Ch. 2] and with no absorption, a solution to (1) is [19]–[21]

$$p_{\mathcal{B}}(t, \boldsymbol{\xi}) = \frac{1}{\sqrt{(2\pi)^n \det(\boldsymbol{\Sigma})}} e^{-\frac{1}{2}(\boldsymbol{\xi} - \boldsymbol{\mu}_{\boldsymbol{\xi}})^{\intercal} \boldsymbol{\Sigma}^{-1} (\boldsymbol{\xi} - \boldsymbol{\mu}_{\boldsymbol{\xi}})}, \tag{2}$$

where $\det(\cdot)$ is the matrix determinant, superscript $\intercal$ is the transpose operator, $\boldsymbol{\mu}_{\boldsymbol{\xi}}$ the mean vector, and $\boldsymbol{\Sigma}$ a covariance matrix.

**Table I**. Human Capillary and BA Emission Parameters [16], [17]

| Parameter (Symbol) | Value | Range |
|---|---|---|
| Blood Mean Velocity $(v_x)$ | 1 $mm/s$ | 0.5-3.3 |
| Capillary Diameter $(L)$ | 8 $\mu m$ | 6-12 |
| Emission Radius $(r)$ | 1 $nm$ | 0.1-500 |

For this paper (2) will later be used to validate numerical methods with $\boldsymbol{\mu}_{\boldsymbol{\xi}} = v_x \cdot t\,[1, 0, 0]^{\intercal} + \boldsymbol{\xi}_0$ and $\boldsymbol{\Sigma} = (2D_B t)\, \boldsymbol{I}$, where $\boldsymbol{I}$ is the identity matrix. Interestingly (2) cannot be used directly to find the so called hit probability

$$\Pr(\exists t > 0 : \mathcal{B}(t) \in \nu_i) \triangleq \Pr(\text{hit } s_i), \tag{3}$$

where $\nu_i$ is a volume occupied by $s_i$ centered at $\boldsymbol{\xi}_i$. Alternatively, the *backward Kolmogorov* equation provides a method to determine (3) with final condition $p_{\mathcal{B}}(t, \boldsymbol{\xi}) = 1_{\nu_i}(\boldsymbol{\xi})$, where $1_{\nu_i}(\boldsymbol{\xi}) = 1$ if $\boldsymbol{\xi} \in \nu_i$ and zero otherwise (e.g., indicator function). However, a closed form analytical solution for (3) is currently unknown. It is possible to estimate (3) using a measure theoretic Martin kernel via [22], [23], [15]

$$\frac{1}{2}\text{Cap}_M(\nu_i) \leq \Pr(\text{hit } s_i) \leq \text{Cap}_M(\nu_i), \tag{4}$$

where for any closed set $\nu_i$ in $\mathbb{R}^d$, $d \geq 3$, $M(\boldsymbol{\xi}_x, \boldsymbol{\xi}_y) = \frac{\|\boldsymbol{\xi}_y\|^{d-2}}{\|\boldsymbol{\xi}_x - \boldsymbol{\xi}_y\|^{d-2}}$ with $\|\boldsymbol{\xi}_x - \boldsymbol{\xi}_y\|$ the Euclidean distance, and

$$\text{Cap}_M(\nu_i) = \left[ \inf_{\mu(\nu_i)=1} \int_{\nu_i} \int_{\nu_i} M(\boldsymbol{\xi}_x, \boldsymbol{\xi}_y)\, d\mu(\boldsymbol{\xi}_x)\, d\mu(\boldsymbol{\xi}_y) \right]^{-1}. \tag{5}$$

Here $\mu(\nu_i)$ is a general Borel measure, not necessarily the Lebesgue measure, so calculating (5) to bound the hit probability in (4) is non-trivial. Additionally, when the nanomachines absorb or impede the flow of a biomarker, then even (1) does not offer a known analytical solution and numerical methods must be applied [19]–[21]. For these reasons, we will use the vector Euler algorithm, which has acceptable strong order and weak order convergence properties [19, Ch. 10] to estimate (3) after using (2) to validate the numerical methods applied within the chosen molecular environment.

### II-C. The Molecular Environment

We consider the *in vivo* environment of a human capillary as discussed in [15] and references therein. The important system model parameters used in this paper are defined in Table I. The biomarkers for this work are assumed to have a radius of 1 nm with an approximated $D_B = 10^{-11}\ \frac{m^2}{s}$, which loosely follows from the *Stokes-Einstein* equation [24] $D_B \leq \frac{K_B T}{6\pi\mu r}$, where $K_B T$ is the thermal energy and $\mu$ is mobility.

Establishing a baseline for evaluation of the Euler algorithm, we use (2) and define

$$f_i(t - t_0) = \int_{\boldsymbol{\xi} \in \nu_i} p_{\mathcal{B}}(t, \boldsymbol{\xi}; \boldsymbol{\xi}_0, t_0)\, d\boldsymbol{\xi},\ t > t_0, \tag{6}$$

to represent the time evolution of the probability a biomarker is within a given volume $\nu_i$. Using the parameters in Table I, Fig. 2 highlights $f_i(t - t_0)$ for a single biomarker and two non-absorbing nanomachines modeled as a cube in $\mathbb{R}^3$ of width, $w = 20$ nm, one centered at $\boldsymbol{\xi}_1 = (50, 0, 0)$ nm and the other at

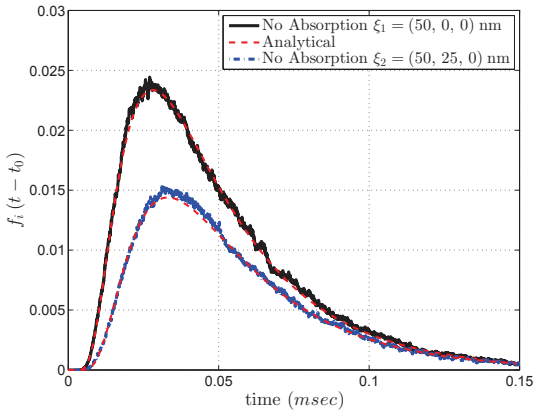


**Fig. 2**. Time evolution probability, $f_i(t - t_0)$ estimated using 10 000 sample paths and the analytical reference per (6), with $D_B = 10^{-11}\ m^2/s$, $v_x = 1\ mm/s$, and $t_0 = 0$ with $s_1$ centered at $\boldsymbol{\xi}_1 = (50, 0, 0)$ nm, and $s_2$ at $\boldsymbol{\xi}_2 = (50, 25, 0)$ nm.

$\boldsymbol{\xi}_2 = (50, 25, 0)$ nm. Notice that the analytical solution using (6) and numerical method are both included in Fig. 2 to highlight the accuracy of the vector Euler algorithm used.

The first-passage, or absorption time for an absorbing boundary, $\boldsymbol{b}$, is defined as $T_{\mathbf{b}}(t) = \inf\{t \geq t_0; \mathcal{B}(t) = \mathbf{b}\}$ [21, pg. 79], which is not equivalent to (3). Solving (1) in $\mathbb{R}^1$ (e.g., 1-D) with drift does offer a closed form pdf of [9], [21, pg. 79]

$$p_{i,b}(t) = \frac{b}{\sqrt{4\pi D_B t^3}} \exp\left(\frac{-(v_x t - b)^2}{4 D_B t}\right), \qquad (7)$$

where $b$ is the *up flow* edge of sensor $s_i$ (e.g., $b = 40$ nm for an $s_i$ of $w = 20$ nm, centered at $\boldsymbol{\xi}_i = (50, 0, 0)$ nm). For reference, a simulation in $\mathbb{R}^1$ (i.e., x-axis) was also done to validate the numerical methods, however, these results are not shown because of space constraints.

Next, a 3-D numerical simulation using the same parameters specified in Fig. 2 was done, but this time assuming only a single sensor that absorbs the biomarker and $\mathbf{b} = \partial\nu_i$ (i.e., the boundary of $\nu_i$), with the experiment repeated at three differing $\boldsymbol{\xi}_i$. These results appear in Fig. 3 with (7) offering an $\mathbb{R}^1$ reference point. As is well known [21, pg. 79], the results for $\boldsymbol{\xi}_2$ and $\boldsymbol{\xi}_3$ depicted in Fig 3 clearly indicate that (7) poorly estimates the $\mathbb{R}^3$ hitting-time pdf and is not entirely applicable to $\mathcal{B}(t) \in \mathbb{R}^3$ for MC based on molecule type (see the constraints these results impose on [9], [11] for an abridged list). In fact, as the nanomachines move farther off the drift axis, the deviation between (7) and the actual pdf becomes increasingly pronounced as one would expect. Notice that $p_{i,\mathbf{b}}(t)$ in $\mathbb{R}^3$ is conditioned on the biomarker hitting $s_i$, an implicit requirement in $\mathbb{R}^1$, and is a condition that significantly impacts MDD as discussed next.

## III. NANOMACHINE DEPENDENT OBSERVATIONS

There are critical differences between MDD analysis and that of traditional wireless DD. Perhaps the biggest difference is that the biomarker and MC channel have the affect known as *channel memory* (see the temporal dependence on $f_i(t - t_0)$ in Fig. 2 and $p_{i,\mathbf{b}}(t)$ in Fig. 3). Another important difference is that a nanomachines biomarkers observation can place both a temporal

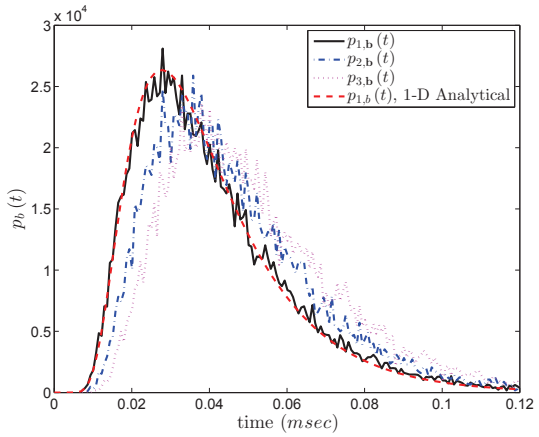


**Fig. 3**. First-hitting time pdf $p_{i,\mathbf{b}}(t)$ in $\mathbb{R}^3$ when $v_x = 1\ mm/s$, $D_B = 10^{-11}\ m^2/s$, $s_1$ centered at $\boldsymbol{\xi}_1 = (50, 0, 0)$ nm with (7) added for reference, $s_2$ at $\boldsymbol{\xi}_2 = (50, 25, 0)$ nm, and $s_3$ at $\boldsymbol{\xi}_3 = (50, 25, 25)$ nm, all modeled as a 20 nm cube.

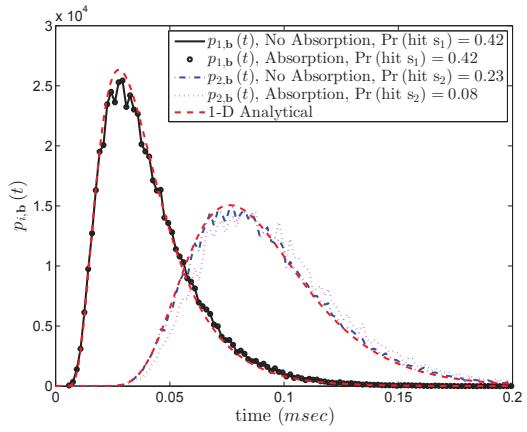


**Fig. 4**. First-hitting time $p_{i,\mathbf{b}}(t)$, indicating spatial dependence among sensors, where $s_1$ is centered at $\boldsymbol{\xi}_1 = (50, 0, 0)$ nm, $s_2$ at $\boldsymbol{\xi}_2 = (100, 0, 0)$ nm, $D_B = 10^{-11}\ m^2/s$, and $v_x = 1\ mm/s$.

and a non-linear spatial dependence on the observations of other nanomachines. For the purposes of this paper, we will assume the nanomachines are fixed in position, resulting in a stationary diffusion process with no temporal dependence. Specifically, if $E_j$ represent a biomarker release at time $t_j$, then $p_{\mathcal{B}}(t, \boldsymbol{\xi}; \boldsymbol{\xi}_0, t_j)$ for $E_j$ is identical to $p_{\mathcal{B}}(t, \boldsymbol{\xi}; \boldsymbol{\xi}_0, t_k)$ associated with $E_k\ \forall j, k$.

Exploring spatial dependence in greater detail, a simulation using two sensors in $\mathbb{R}^3$, both located along the x-axis was done. These results appear in Fig. 4 with the simulation parameters listed in the figure caption. There are four key aspects on display in Fig. 4. First, $p_{i,\mathbf{b}}(t)$ is shown for a non-stopping time (No Absorption), a stopping-time (Absorption), and the 1-D analytical reference solution using (7). Second, the biomarker Pr (hit $s_i$) is displayed in the figure legend. Third, the down-flow sensor $s_2$ is clearly spatially dependent on the up-flow sensor $s_1$, with Pr (hit $s_2$) decreasing by a factor of three if $s_1$ influences (absorbs) the biomarker. Additionally, $p_{2,\mathbf{b}}(t)$ with absorption, is slightly shifted to the

right in time, representing the "longer" path a biomarker must take to pass around $s_1$, while interestingly, the shape of the pdf is little changed. Forth, the up-flow sensor $s_1$ is not influenced by the down-flow sensor $s_2$ (i.e., non-linear spatial dependence). One additionally complexity of MDD relative to traditional DD theory is that some biomarkers (e.g., VEGF) occur naturally, denoted by $F_i$. Clearly, when the disease is absent, this phenomenon results in a non-zero $\Pr(\text{hit } s_i)$, leading to a type I error. At the same time, a sensor may detect a naturally occurring biomarker when the disease is present, adding complexity to the type II error analysis.

## IV. DATA FUSION

With an understanding of the hit probability for both independent and spatially dependent nanomachine observations, we now shift gears and explore MDD data fusion at the FC. When a single disease is to be detected, MDD can be formulated as a binary hypothesis testing problem with $\mathcal{H}_1$ : disease present, and $\mathcal{H}_0$ : disease absent. All $N$ nanomachines deciding locally $\mathcal{H}_1$ or $\mathcal{H}_0$ and forward this decision to the FC in a parallel fashion (see Fig. 1) either using MC or acoustically. Establishing a statistical framework, let each local decision received at the FC be represented as a random variable, $U_i$, with possible realizations of $u_i = 1$ for $\mathcal{H}_1$ or $u_i = 0$ for $\mathcal{H}_0$. The false alarm probability, $p_{fa,i} = \Pr(U_i = 1 \,|\, \mathcal{H}_0)$ can be determined analytically or estimated, while the detection probability, $p_{d,i} = \Pr(U_i = 1 \,|\, \mathcal{H}_1)$ depends on both naturally occurring and disease generated biomarkers. Specifically,

$$p_{d,i} = \Pr(B_i) + \Pr(F_i) - \Pr(B_i)\Pr(F_i),$$

by the inclusion-exclusion principle, assuming the naturally occurring and disease generated biomarkers events are independent, where event $B_i$ represents the latter biomarker.

Even under the assumption of spatially independent observations, determination of $p_{fa,i}$ and $p_{d,i}$ $\forall i$ appears formidable in an *in vivo* environment. However, should these values be available via calculation or numerical analysis (e.g., genie aided analysis) a bound on detection performance can be obtained using the optimal *Chair-Varshney (CV)* fusion rule for conditionally independent observations [25]

$$\Lambda = \log\frac{\Pr(\mathcal{H}_1|\boldsymbol{u})}{\Pr(\mathcal{H}_0|\boldsymbol{u})} = \log\frac{\pi_1}{\pi_0} + \sum_{i=1}^{N} u_i \log\frac{p_{d,i}}{p_{fa,i}} + \sum_{i=1}^{N}(1-u_i)\log\frac{1-p_{d,i}}{1-p_{fa,i}} \underset{\mathcal{H}_0}{\overset{\mathcal{H}_1}{\gtrless}} \ell, \tag{8}$$

where $\Lambda$ is a sufficient statistic, $\boldsymbol{u} = \{u_1, u_2, \ldots, u_N\}$ are the realizations of each $U_i$, $\pi_1 = \Pr(\mathcal{H}_1)$ and $\pi_0 = \Pr(\mathcal{H}_0)$, and $\ell$ is a threshold chosen to meet a desired performance goal(s). Because determination of (8) is so problematic *in vivo*, an alternative suboptimal fusion rule is the counting or $K$ out of $N$ fusion rule

$$\Lambda_c = \sum_{i=1}^{N} u_i \underset{\mathcal{H}_0}{\overset{\mathcal{H}_1}{\gtrless}} K, \tag{9}$$

which simply counts the total number of observations and compares that value to a threshold $K$.

When the observations are spatially dependent, then a more complex analysis is required. Standardizing on notation common to hypothesis testing problems, suppose $X_i$ is the event that a biomarker hits sensor $s_i$ and that $X_i$ has a temporal pdf given hypothesis $\mathcal{H}_j$ and emission rate $\kappa_j$ of $p_{X_i}(x_i|\mathcal{H}_j, \kappa_j)$. Notice that $\kappa_j$ represents the effective biomarker emission rates with and without the disease present. Then for spatially dependent observations, the joint pdf

$$p_{\boldsymbol{X}}(x_1, x_2, \ldots, x_N|\mathcal{H}_j, \kappa_j) \neq \prod_{i=1}^{N} p_{X_i}(x_i|\mathcal{H}_j, \kappa_j), \tag{10}$$

which is evidenced by the results in Fig. 4. Improved detection performance follows from the generalized likelihood ratio test (GLRT)

$$L(\boldsymbol{X}) = \frac{\pi(\hat{\kappa}_1)\, p_{\boldsymbol{X}}(\boldsymbol{x}|\mathcal{H}_1, \hat{\kappa}_1)}{\pi(\hat{\kappa}_0)\, p_{\boldsymbol{X}}(\boldsymbol{x}|\mathcal{H}_0, \hat{\kappa}_0)} \underset{\mathcal{H}_0}{\overset{\mathcal{H}_1}{\gtrless}} \gamma, \tag{11}$$

where the maximum *a posteriori* (MAP) estimate is

$$\hat{\kappa}_j = \arg\max_{\kappa_j} \pi(\kappa_j)\, p_{\boldsymbol{X}}(\boldsymbol{x}|H_j, \kappa_j), \; j = 0, 1.$$

However, determination of $p_{\boldsymbol{X}}(\boldsymbol{x}|\mathcal{H}_j, \hat{\kappa}_1)$ in (11) is complex because of (10). Perhaps the statistical theory of copulas may be useful in studying (11) given its ability to estimate a joint pdf when the observations are non-linearly spatially dependent [26]. Nevertheless, we show the receiver operating characteristic (ROC) curves for randomly located set of senors in a cone pattern using fusion rules (8) and (9) if the observations are independent, and again using (9) when the observations are spatially dependent in Fig. 5. Notice that when the observations are spatially dependent, the detection performance of the counting rule fusion drops significantly, representing an interesting open MDD research topic.

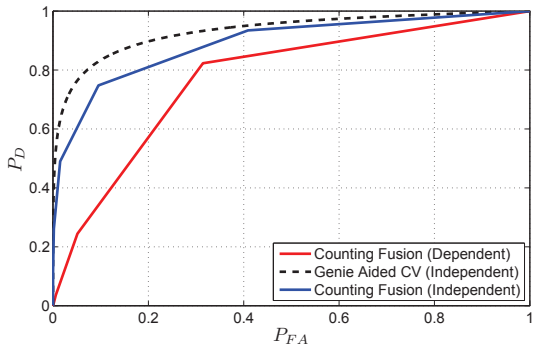


**Fig. 5**. ROC curves comparing the *CV,* (8), and the *counting* fusion, (9), rules against the *counting* fusion rule with spatially dependent observations using monte-carlo simulation with 2 000 iterations, where $N = 30$, $p_{fa,i} \triangleq \frac{1}{5}\bar{p}_d \; \forall i$ with $\bar{p}_d = \frac{1}{N}\sum_{i=1}^{N} p_{d.i}$, and each $p_{d,i}$ is determined numerically.

## V. CONCLUSIONS

A Brownian motion model for biomarker propagation and MDD by a collection of nanomachines was presented. It was shown that the observations are spatially dependent in a non-linear fashion, and that this effect opens new and interesting research opportunities, such as the need for a $\mathbb{R}^3$ hitting-time model, a copula based GLRT, and a tractable *in vivo* fusion rule.

## VI. REFERENCES


[1] P. Couvreur and C. Vauthier, "Nanotechnology: Intelligent design to treat complex disease," *Pharmaceutical Research*, vol. 23, no. 7, pp. 1417–1450, 2006.

[2] A. Cavalcanti, B. Shirinzadeh, R. A. F. Jr, and T. Hogg, "Nanorobot architecture for medical target identification," *Nanotechnology*, vol. 19, no. 1, p. 015103, 2008.

[3] V. Denes, M. Lakk, A. Makarovskiy, P. Jakso, S. Szappanos, L. Graf, L. Mandel, I. Karadi, and P. Geck, "Metastasis blood test by flow cytometry: In vivo cancer spheroids and the role of hypoxia," *International Journal of Cancer*, vol. 136, no. 7, pp. 1528–1536, 2015.

[4] T. Nakano, A. W. Eckford, and T. Haraguchi, *Molecular Communication*. Cambridge University Press, 2013.

[5] V. Loscri and A. Vegni, "An acoustic communication technique of nanorobot swarms for nanomedicine applications," *IEEE Trans. Nanobiosci.*, vol. 14, no. 6, pp. 598–607, Sept 2015.

[6] National Cancer Institute. (2016, July) Learn about nanotechnology in cancer. [Online]. Available: http://nano.cancer.gov/learn/index.asp

[7] F. Dressler and O. Akan, "Bio-inspired networking: from theory to practice," *IEEE Commun. Soc. Mag.*, vol. 48, no. 11, pp. 176–183, November 2010.

[8] T. Nakano, M. Moore, F. Wei, A. Vasilakos, and J. Shuai, "Molecular communication and networking: Opportunities and challenges," *IEEE Trans. Nanobiosci.*, vol. 11, no. 2, pp. 135–148, June 2012.

[9] S. Kadloor, R. Adve, and A. Eckford, "Molecular communication using brownian motion with drift," *IEEE Trans. Nanobiosci.*, vol. 11, no. 2, pp. 89–99, June 2012.

[10] N.-R. Kim and C.-B. Chae, "Novel modulation techniques using isomers as messenger molecules for nano communication networks via diffusion," *IEEE J. Sel. Areas Commun.*, vol. 31, no. 12, pp. 847–856, December 2013.

[11] N.-R. Kim, A. Eckford, and C.-B. Chae, "Symbol interval optimization for molecular communication with drift," *IEEE Trans. Nanobiosci.*, vol. 13, no. 3, pp. 223–229, Sept 2014.

[12] T. Nakano, T. Suda, Y. Okaie, M. Moore, and A. Vasilakos, "Molecular communication among biological nanomachines: A layered architecture and research issues," *IEEE Trans. Nanobiosci.*, vol. 13, no. 3, pp. 169–197, Sept 2014.

[13] M. O. Stefanini, F. T. Wu, F. Mac Gabhann, and A. S. Popel, "A compartment model of VEGF distribution in blood, healthy and diseased tissues," *BMC Systems Biology*, vol. 2, no. 1, pp. 1–25, 2008.

[14] N. R. Raz, M. R. Akbarzadeh-T., and M. Tafaghodi, "Bioinspired nanonetworks for targeted cancer drug delivery," *IEEE Trans. Nanobiosci.*, vol. 14, no. 8, pp. 894–906, Dec 2015.

[15] U. Rogers and M. S. Koh, "Parallel molecular distributed detection with brownian motion," *IEEE Trans. Nanotechnol.*, vol. in press, no. 99, Dec 2016.

[16] H. N. Mayrovitz, D. Larnard, and G. Duda, "Blood velocity measurement in human conjunctival vessels," *Cardiovascular diseases*, vol. 8, no. 4, pp. 509–526, 1981.

[17] A. G. Koutsiaris, S. V. Tachmitzi, P. Papavasileiou, N. Batis, M. G. Kotoula, A. D. Giannoukas, and E. Tsironi, "Blood velocity pulse quantification in the human conjunctival precapillary arterioles," *Microvascular Research*, vol. 80, no. 2, pp. 202 – 208, 2010.

[18] J. Tan, A. Thomas, and Y. Liu, "Influence of red blood cells on nanoparticle targeted delivery in microcirculation," *Soft Matter*, vol. 8, pp. 1934–1946, 2012.

[19] C. W. Gardiner, *Handbook of stochastic methods for physics, chemistry and the natural sciences*. Springer-Verlag, 2004.

[20] J. K. Dhont, *An introduction to dynamics of colloids*. Elsevier, 1996.

[21] I. Karatzas and S. S. E., *Brownian motion and stochastic calculus*, 2nd ed. Springer-Verlag, New York Inc., 1991.

[22] Y. P. Itai Benjamini, Robin Pemantle, "Martin capacity for markov chains," *The Annals of Probability*, vol. 23, no. 3, pp. 1332–1346, 1995.

[23] P. Mörters and Y. Peres, *Brownian motion*. Cambridge University Press, 2010, vol. 30.

[24] "Molecular volumes and the stokes-einstein equation," *Journal of Chemical Education*, vol. 47, no. 4, p. 261, 1970.

[25] Z. Chair and P. Varshney, "Optimal data fusion in multiple sensor detection systems," *IEEE Trans. Aerosp. Electron. Syst.*, vol. AES-22, no. 1, pp. 98 –101, Jan. 1986.

[26] R. B. Nelsen, *An introduction to copulas*, 2nd ed. Springer Science+Business Media, Inc., 2007.